Melting behavior of Ag14 cluster: An order parameter by instantaneous normal modes

Ping-Han Tang, Ten-Ming Wu, P. J. Hsu, and S. K. Lai

Articles you may be interested in

How a single aluminum atom makes a difference to gallium: First-principles simulations of bimetallic cluster melting
J. Chem. Phys. **139**, 094309 (2013); 10.1063/1.4819907

Comparative study of cluster Ag17Cu2 by instantaneous normal mode analysis and by isothermal Brownian-type molecular dynamics simulation
J. Chem. Phys. **135**, 094302 (2011); 10.1063/1.3628669

Melting scenario in metallic clusters
J. Chem. Phys. **129**, 194302 (2008); 10.1063/1.3009194

First-principles investigation of finite-temperature behavior in small sodium clusters
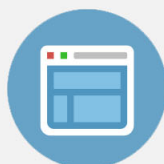J. Chem. Phys. **123**, 164310 (2005); 10.1063/1.2076607

Specific heat and Lindemann-like parameter of metallic clusters: Mono- and polyvalent metals
J. Chem. Phys. **121**, 1487 (2004); 10.1063/1.1763144

Melting behavior of Ag$_{14}$ cluster: An order parameter by instantaneous normal modes

Ping-Han Tang,[1] Ten-Ming Wu,[1,a)] P. J. Hsu,[2,3] and S. K. Lai[2,3,b)]

[1]*Institute of Physics, National Chiao-Tung University, Hsinch 300, Taiwan*
[2]*Complex Liquids Laboratory, Department of Physics, National Central University, Chungli 320, Taiwan*
[3]*Molecular Science and Technology Program, Taiwan International Graduate Program, Academia Sinica, Taipei 115, Taiwan*

This paper studies the melting behavior of Ag$_{14}$ cluster employing the instantaneous normal mode (INM) analysis that was previously developed for bimetallic cluster Ag$_{17}$Cu$_2$. The isothermal Brownian-type molecular dynamics simulation is used to generate atom configurations of Ag$_{14}$ at different temperatures up to 1500 K. At each temperature, these atomic configurations are then analyzed by the INM technique. To delve into the melting behavior of Ag$_{14}$ cluster which differs from Ag$_{17}$Cu$_2$ by the occurrence of an anomalous prepeak in the specific heat curve in addition to the typical principal peak, we appeal to examining the order parameter $\tau(T)$ defined in the context of the INM method. Two general approaches are proposed to calculate $\tau(T)$. In one, $\tau(T)$ is defined in terms of the INM vibrational density of states; in another, $\tau(T)$ is defined considering the cluster as a rigid body with its rotational motions described by three orthogonal eigenvectors. Our results for Ag$_{14}$ by these two methods indicate the mutual agreement of $\tau(T)$ calculated and also the consistent interpretation of the melting behavior with the specific heat data. The order parameter $\tau(T)$ provides in addition an insightful interpretation between the melting of clusters and the concept of broken symmetry which has been found successful in studies of the melting transition of bulk systems. © *2012 American Institute of Physics.* [http://dx.doi.org/10.1063/1.4772096]

I. INTRODUCTION

A general description of the melting transition in a cluster from the solid-like to liquid-like phase is far more complicated than its bulk counterpart.[1] Due to their finite sizes, the kind of sharp transition at a well-defined melting temperature often observed in bulk systems has been replaced in clusters by a more gradual transition that spans a temperature range. This finite-size-effect transition has been predicted to scale as the inverse of the cluster particle number.[2,3] The specific heat C_V is by far still the most frequently used quantity to feature the melting transition of clusters. Differing from the bulk system where there is a discontinuous jump at the melting point, the temperature variation of C_V in a cluster may exhibit a single principal or main peak with perhaps a prepeak appearing at a lower temperature.[4–11] In either a bulk or a cluster, the melting temperature T_m is customarily defined as the position of the main peak.

A microscopic understanding of the melting transition in a cluster requires an order parameter that manifests its structural change from the solid-like to liquid-like phase. In the literature, such microscopic order parameters have indeed been proffered. The short-time average of temperature in the microcanonical ensemble provides a concrete evidence for the coexistence of isomers that were found to assume the solid-like and liquid-like phases within a temperature range and one quite often specifies the coexistence as a signature of cluster melting.[12–15] Structures of the clusters in the coexistence region were analyzed also by the method of common neighbor pairs.[16] Another quantity is the potential energy function commonly used for addressing the transition between two coexistence cluster isomers that are individually stable in the Landau free energy but are separated by an energy barrier.[17] There are, moreover, some geometric order parameters that are applied to characterize transition between two stable isomers and their coexistence,[18] and these order parameters are calculated on the basis of the short-time average in simulations. An approach along the same line is the bond-orientational order parameter which is applied to investigate the structural variation of clusters along pathways in configuration space.[19,20] The structural transitions of clusters are recently understood by using simultaneously two bond-orientational order parameters.[21,22] Analogous to the Lindemann parameter used for bulk systems, the root-mean-square bond length fluctuation constant δ continues receiving much attention in computer simulations. We note, however, that this parameter does not work so well for clusters.[10,23,24]

Very recently, we have studied the dynamics and the melting behavior of Ag$_{17}$Cu$_2$ from the viewpoint of potential energy landscape[25,26] by exploiting the INM analysis[27,28] in the context of the canonical ensemble average. In that work, a new order parameter was proposed in terms of the INM vibrational density of states (DOS) that are associated with the Ag atoms in the cluster.[29] This order parameter interprets pretty well the melting behavior of Ag$_{17}$Cu$_2$ and the predicted T_m is in fairly good agreement with that inferred from C_V.[30]

a)tmw@faculty.nctu.edu.tw.
b)sklai@coll.phy.ncu.edu.tw.

In this paper, we study the melting transition of metallic cluster Ag_{14} based on a generalization of the INM analysis which will be described in Sec. III. The main difference in the melting behavior between Ag_{14} and $Ag_{17}Cu_2$ clusters lies in the temperature variation of their C_V which both possess a main maximum but the C_V of Ag_{14} exhibits in addition a prepeak at a lower temperature. It is found furthermore that the structures of the two clusters at their respective lowest-energy state (LES) are quite different geometrically. The LES of $Ag_{17}Cu_2$ consists of the 19-atom double icosahedron, which may be viewed as two interpenetrating 13-atom icosahedrons with two Cu atoms at the centers. The LES of Ag_{14}, however, comprises an icosahedron and one floating atom (or adatom) residing outside. According to our previous studies of Cu_{14}[11] whose C_V also shows a main peak and a prepeak as that of Ag_{14}, the origin of the prepeak is due to the migrational relocation of the floating atom in the cluster as the temperature of the cluster is raised from the LES.

This paper is organized as follows. In Sec. II, we give a brief description of the isothermal Brownian-type molecular dynamics (MD) simulation technique and introduce the Gupta empirical potential that was used to account for interparticle interactions in simulations. The generation of atom configurations for Ag_{14} at each temperature, the result of C_V and the appearance of the cluster excited states with increasing temperature are also summarized. In the same section, we present as well the structure and vibrational modes of the cluster at its LES. In Sec. III, the INM analysis for clusters is first described briefly. Then, we address analytically two different ways of defining the order parameter by either the INM vibrational DOS of individual atoms or the purely rotational modes of the whole cluster. In Sec. IV, our calculated results of Ag_{14} are presented and we show numerically that the two approaches for defining the order parameter dictate almost equivalent results. A conclusion of our work is given in Sec. V.

II. SIMULATION, THERMAL PROPERTIES, AND LOWEST-ENERGY STRUCTURE

A. Simulation

In this paper, the isothermal Brownian-type MD simulation is applied to generate the cluster configurations of Ag_{14} at different temperatures. The considerable technical details of the simulation are well documented in Refs. 10, 11, and 24, to which the interested readers are referred. As in one of our previous works for Ag-based cluster,[30] we employ the empirical *n*-body Gupta potential[31] which reads

$$E_n = \sum_{i=1}^{n} [V_r(i) - (V_a(i))^{1/2}],   (1)$$

where *n* is the number of particles in the cluster, the repulsive term V_r is

$$V_r(i) = A \sum_{j \neq i}^{n} \exp\left[-p\left(\frac{r_{ij}}{r_0} - 1\right)\right]   (2)$$

and the attractive term V_a, due to the hybridization of valence electrons, is

$$V_a(i) = \varsigma^2 \sum_{j \neq i}^{n} \exp\left[-2q\left(\frac{r_{ij}}{r_0} - 1\right)\right].   (3)$$

The parameters A, p, q, ς, and r_0 have been determined by fitting to measured bulk values. For the metal Ag, these parameters are taken from Rapallo *et al.*[32] and they are $A = 0.1031$ eV, $\varsigma = 1.1895$ eV, $p = 10.85$, $q = 3.180$, and $r_0 = 2.89$ Å.

The lowest energy structure of the cluster is searched by a technique described in Refs. 30 and 33. Beginning at the LES, the cluster at a finite temperature can be prepared by the MD run, in which the cluster temperature is raised gradually from zero.[24,29] In all of these simulations, atoms at a finite temperature are traced by their labels which are tagged at their LES.

B. Thermal properties

Following our previous works,[10,24] we calculate C_V via the following formula:

$$C_V = \frac{\langle E_{total}^2 \rangle_t - \langle E_{total} \rangle_t^2}{k_B T^2},   (4)$$

where E_{total} includes the total kinetic energy plus the potential energy E_n given in Eq. (1) and $\langle \dots \rangle_t$ means taking the time average (see Eq. (10) in Ref. 24). The calculated C_V of Ag_{14} has been shown previously in Fig. 1 of Ref. 30. As shown there, the main maximum of C_V, which is defined as the melting temperature T_m, is located at approximately 920 K. Besides the main peak, one notices a prepeak structure near 300 K. In the temperature range $0 < T \leq 500$ K, we present also the cluster's excited states by an energy histogram.[30] For $T < 140$ K, the cluster is only found in the LES. The first excited state of the cluster first appears near 150 K and by 200 K the second excited state emerges. At $T = 500$ K, higher excited states of the cluster are seen.

C. Lowest-energy structure

The LES of Ag_{14} consists of an icosahedron and a floating atom which is located outside it at an equal distance from three atoms that form a triangular facet of the icosahedron. The icosahedron is not perfect but a slightly deformed one, which will be evidenced later. By removing away the floating atom, the deformed icosahedral geometry can be relaxed into a perfect icosahedron whose surface consists of 20 identical equilateral triangular facets with a bond-length side of 2.689 Å. By comparing the structure of this perfect icosahedron with the deformed one in Ag_{14}, we find that their major difference lies in the very small expansion of the triangular facet capped on top by the floating atom and the expanded triangular facet is still equilateral but now having a bond-length of 2.705 Å.

Differing from the perfect icosahedron which has the I_h point group symmetry, the geometric structure of the LES of Ag_{14} takes on the C_{3v} point group with the principal axis
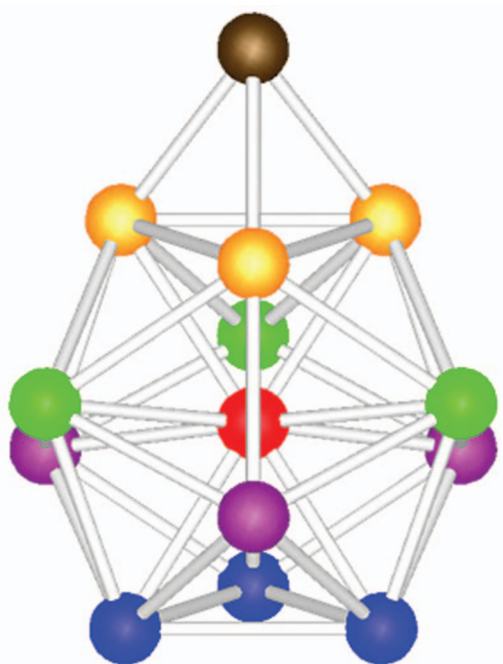
FIG. 1. Six subsets of atoms of Ag$_{14}$ in the LES. The atoms of the cluster are classified into two single-atom subsets, the *C* (red) and *F* (brown) atoms, and four three-atom subsets, the S_1 (orange), S_2 (green), S_3 (violet), and S_4 (blue) atoms, which are at distances 2.681, 4.579, 5.438, and 6.573 Å from the *F* atom, respectively.

FIG. 2. Vibrational frequencies of Ag clusters: (a) the LES of Ag$_{14}$, (b) the deformed icosahedron obtained by removing away the *F* atom from the LES, (c) the perfect icosahedron obtained by relaxing the deformed icosahedron. In each panel, the blue straight lines indicate the frequencies of the vibrational modes and the red dots specify the degeneracies of the modes.

passing through the central atom inside the icosahedron and the adatom.[34] The 12 atoms at the vertices of the deformed icosahedron can be recognized as four equilateral triangles on four different planes perpendicular to this principal axis, and that the three atoms of each equilateral triangle have an equal distance from the floating atom. Thus, the 14-atom Ag$_{14}$ in its LES has a three-fold rotational symmetry about the principal axis and a reflection symmetry about the plane containing the principal axis and anyone of the 12 atoms. According to the C_{3v} point group, atoms of the LES of Ag$_{14}$ are classified into six subsets, which are shown in Fig. 1. The central atom and the floating atom are two subsets each of single atom and are denoted hereafter as *C* and *F*, respectively. The other 12 atoms are differentiated into four subsets, with each subset containing the three atoms consisting of one equilateral triangle mentioned above. With distances from the *F* atom at 2.681, 4.579, 5.438, and 6.573 Å, the four subsets of atoms are S_1, S_2, S_3, and S_4 representing from the nearest to the farthest distance, respectively.

Several theoretical studies on the structures and the vibrational modes of metallic clusters that employ the Gupta potential have been reported in the literature.[35,36] Depicted in Fig. 2(a) are the vibrational modes of Ag$_{14}$ in the LES. Due to the C_{3v} symmetry, the vibrational frequencies are either nondegenerate or doubly degenerate. Removing away the *F* atom, we also calculate and compare the vibrational modes of the deformed icosahedron and the relaxed perfect one and these latter two results are shown in Figs. 2(b) and 2(c), respectively. As indicated by the degeneracies of the vibrational modes, the deformed icosahedron reflects the symmetry of the C_{3v} point group, whereas the relaxed icosahedron, with the I_h
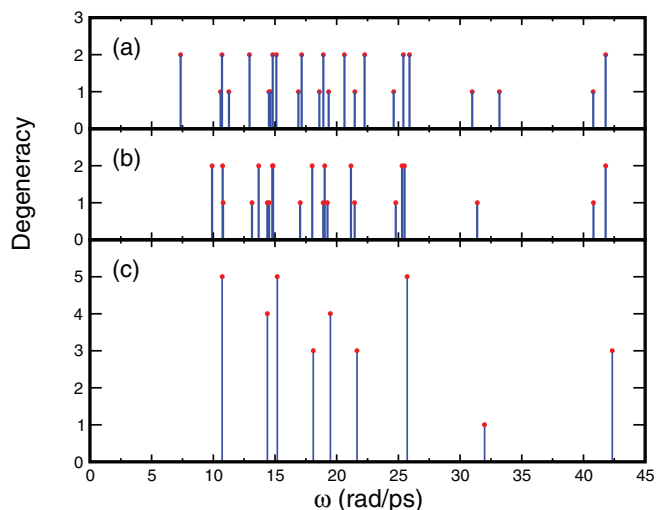
symmetry, correctly produces the vibrational modes with five-fold, fourfold, and threefold degeneracies.[35]

Some vibrational modes of Ag$_{14}$ are interesting. The three highest-frequency modes, the singlet at 40.8 rad/ps and the doublet at 41.8 rad/ps, generally describe the *C*-atom in-side the deformed icosahedron oscillating parallel and per-pendicular to the principal axis, respectively. The singlet at 31 rad/ps is the breathing mode, describing the motion of atoms along lines from the atoms to the *C*-atom. Comparing the vibrational modes of the Ag clusters with and without the *F* atom, we find three extra modes due to the presence of the *F* atom and they are the singlet at 33.2 rad/ps and the dou-blet at 7.35 rad/ps, which describe generally the stretching and shearing vibrations between the *F* atom and the deformed icosahedron, respectively. The other modes with frequencies 10–26 rad/ps mainly come from the vibrational modes of the perfect icosahedron, with a reduction in some degeneracies due to the change in group symmetry from I_h to C_{3v} and a shift in their frequencies by the presence of the *F* atom.

III. INSTANTANEOUS NORMAL MODE ANALYSIS FOR CLUSTERS

In a series of three papers, Adam and Stratt[37–39] advanced the general idea of exploiting INM analysis for clusters. This strategy was generalized, somewhat quantitatively, by Tang *et al.*[29] to bimetallic clusters, studying their dynamics and their melting behavior. In this section, we give a brief review of the methodology and apply it below to a cluster of *n* identical atoms whose interparticle interactions are described by the empirical many-body Gupta potential. Evaluated at given configuration of *n* atoms in the Cartesian position coordinates specified by the 3*n*-dimensional vector $\boldsymbol{R} = (r_{1,x}, r_{1,y}, r_{1,z}, \ldots, r_{n,x}, r_{n,y}, r_{n,z})$, the mass-weighted Hessian matrix $\boldsymbol{K}(\boldsymbol{R})$

can be calculated by the formula[39]

$$K_{i\mu,j\nu}(\boldsymbol{R}) = \frac{1}{m}\left(\frac{\partial^2 V(\boldsymbol{R})}{\partial r_{i\mu}\partial r_{j\nu}}\right), \qquad (5)$$

where m is the atom mass, and $V(\boldsymbol{R})$ is the total potential energy of the cluster (which is E_n for Gupta potential), and the subscript $i\mu$ ($j\nu$) refers to atom i (j) with $\mu = x, y, z$ ($\nu = x, y, z$). The analytic formula for the elements of the Hessian matrix derived for the Gupta potential are well documented in Ref. 29. The eigenmodes of the $3n \times 3n$ matrix $\boldsymbol{K}(\boldsymbol{R})$ are referred to as the INMs at configuration $\boldsymbol{R}$. Since the configuration $\boldsymbol{R}$ at which the INMs are evaluated may not correspond to a local minimum of $V(\boldsymbol{R})$, the INM frequencies ω_α, $\alpha = 1, \ldots, 3n$, which are the square-root of the eigenvalues of $\boldsymbol{K}(\boldsymbol{R})$, may be either real or imaginary. The αth normalized INM eigenvector is expressed by the three-dimensional displacements $\vec{e}_j^{\,\alpha}$, where $j = 1, \ldots, n$ for all atoms.

A. Rotational INMs

In an n-atom cluster, besides the three INMs with zero eigenvalue, which correspond to the translational motions of the center-of-mass, the remaining $3n$-3 INMs describe the instantaneous rotational motions of the whole cluster and the instantaneous vibrations of atoms. At given instant, one can sort out the degrees of freedom associated with the rotational motions of the whole cluster by the following two methods:[26,36]

(1) *Method I:* The cluster at given instant is treated as a rigid body. Based on the conservation of the total angular momentum,[40] the normalized eigenvectors of the three purely rotational modes, denoted as (R_x, R_y, R_z), of a cluster at a configuration $\boldsymbol{R}$ can be expressed as[29,41]

$$\vec{e}_j^{\,R_x} = \sqrt{\frac{m}{I_x}}\begin{pmatrix} 0 \\ -r'_{jz} \\ r'_{jy} \end{pmatrix}, \quad \vec{e}_j^{\,R_y} = \sqrt{\frac{m}{I_y}}\begin{pmatrix} r'_{jz} \\ 0 \\ -r'_{jx} \end{pmatrix},$$

$$\vec{e}_j^{\,R_z} = \sqrt{\frac{m}{I_z}}\begin{pmatrix} -r'_{jy} \\ r'_{jx} \\ 0 \end{pmatrix}, \quad j = 1, \ldots, n, \qquad (6)$$

where $r'_{j\mu}$ ($\mu = x, y, z$) are the Cartesian position coordinates of the jth atom in the body frame of the cluster whose origin is chosen at the center-of-mass. In this body frame, the coordinate axes coincide with the principal axes of the cluster. With respect to each one of the three principal axes, the moment of inertia I_μ is defined as

$$I_\mu = m\sum_{j=1}^n\left(r'^2_{j\nu} + r'^2_{j\eta}\right), \qquad (7)$$

where $\mu \neq \nu \neq \eta$ which we assume them cyclic in x, y, and z. In this Method I, the rotational and vibrational degrees of freedom at an instant are assumed to be completely decoupled. The three purely rotational eigenvectors are mutually orthonormal and they form a set of basis vectors in the three-dimensional subspace which are used to describe the rotational degrees of freedom of a cluster configuration at given instant. However, one should notice that the purely rotational

bases of cluster configurations at two successive instants may not be transformable by merely rotating the principal axes of the cluster in a real space. The reason is that there exists in a cluster the inherent rotation-vibration couplings which may cause a mixing between the instantaneous subspaces of the rotation and vibration from one instant to the next. Thus, this method generally works well for clusters in which the rotation-vibration couplings are extremely weak.

(2) *Method II:* Strictly speaking, the three purely rotational eigenvectors are not the eigenmodes of the Hessian matrix $\boldsymbol{K}(\boldsymbol{R})$ but approximate ones when the rotation-vibration couplings become significant. In an approximate scheme, it has been proposed that the rotational degrees of freedom of a cluster configuration can be brought near to the three INMs by sorting out the largest angular momentum values.[36] We denote these three INMs as (L_1, L_2, L_3). The instantaneous cluster rotations are again described, quite generally, by the three rotational INMs, although they are hybridized with the vibrational degrees of freedom and the extent of the hybridization increases with temperature. This will be shown later.

The three INM eigenvectors associated with (L_1, L_2, L_3) of a cluster are orthonormal and also form a three-dimensional subspace in the fully $3n$-dimensional configuration space of the cluster. To examine the overlap between the subspace spanned by the INM eigenvectors of (L_1, L_2, L_3) and that by the eigenvectors of the purely rotational modes (R_x, R_y, R_z), we define the following quantity:

$$J(L_k) = \left\langle \sum_{\eta=x,y,z}\left(\sum_{j=1}^n \vec{e}_j^{\,L_k}\cdot\vec{e}_j^{\,R_\eta}\right)^2\right\rangle, \quad k=1,2,3, \qquad (8)$$

where the brackets $\langle\ldots\rangle$ mean an ensemble average over cluster configurations. As so defined, $J(L_k)$ measures the projection of the rotational INM eigenvector $\vec{e}_j^{\,L_k}$ onto the subspace spanned by the eigenvectors of the purely rotational modes (R_x, R_y, R_z). Note that the two subspaces are completely overlapped whenever $J(L_k) = 1$, $k = 1, 2, 3$, whereas for $J(L_k) < 1$ the eigenvector $\vec{e}_j^{\,L_k}$ hybridizes with the degrees of freedom of the vibrational INMs and the two subspaces are not completely overlapped; the less the value of $J(L_k)$ is, the stronger is the hybridization.

B. Ensemble-averaged projection

By excluding the three-translational and three-rotational INMs, an ensemble average of the INM vibrational DOS is defined as[29,39]

$$D_{Vib}(\omega) = \left\langle \frac{1}{3n-6}\sum_{\alpha=1}^{3n-6}\delta(\omega-\omega_\alpha)\right\rangle \qquad (9)$$

with the DOS being normalized. Generally, $D_{Vib}(\omega)$ composes of two lobes which are $D^{(s)}(\omega)$, the DOS of the stable INMs (denoted by the superscript s) with real frequencies ω, and $D_{Vib}^{(u)}(\lambda)$, the DOS of the unstable INMs (denoted by the superscript u) with imaginary frequencies $\omega_\alpha = i\lambda_\alpha$. The normalization of $D_{Vib}(\omega)$ yields a unit area under the curves of $D_{Vib}^{(s)}(\omega)$ and $D_{Vib}^{(u)}(\lambda)$, which are plotted in the positive and negative axes of ω, respectively.[42,43]

For a single cluster configuration, the projection operator $\hat{P}_j^\alpha$ of atom j in the αth INM is given in the literature[44,45] as

$$\hat{P}_j^\alpha = |\vec{e}_j^\alpha|^2 = \sum_{\mu=x,y,z} e_{j\mu}^\alpha e_{j\mu}^\alpha. \tag{10}$$

With $\hat{P}_j^\alpha$, we may calculate the contribution of each atom to the INM vibrational DOS according to the definition

$$D_j(\omega) = \frac{1}{3N-6} \left\langle \sum_{\alpha=1}^{3N-6} \hat{P}_j^\alpha \delta(\omega - \omega_\alpha) \right\rangle. \tag{11}$$

$D_{Vib}(\omega)$ in Eq. (9) is thus a sum of $D_j(\omega)$ over *all* atoms in the cluster. By the completeness of all INM eigenvectors, the projection operators of an atom in a configuration obey the following sum rule:

$$\hat{P}_j^T + \hat{P}_j^R + \sum_{\alpha=1}^{3n-6} \hat{P}_j^\alpha = 3 \tag{12}$$

with

$$\hat{P}_j^T \equiv \hat{P}_j^{T_x} + \hat{P}_j^{T_y} + \hat{P}_j^{T_z} \tag{13}$$

and

$$\hat{P}_j^R \equiv \hat{P}_j^{L_1} + \hat{P}_j^{L_2} + \hat{P}_j^{L_3}, \tag{14}$$

where (T_x, T_y, T_z) and (L_1, L_2, L_3) are the three translational and rotational INMs according to *Method II*, respectively. To proceed further, we define a useful quantity I_j of atom j and refer it as an ensemble average of all vibrational $\hat{P}_j^\alpha$ associated with the atom. Accordingly, the I_j of a cluster at a finite temperature can be calculated by two averages, first averaging the $3n$-6 vibrational $\hat{P}_j^\alpha$ at a configuration of the cluster, and then over all possible configurations generated by simulations, i.e.,

$$I_j = \left\langle \frac{1}{3n-6} \sum_{\alpha=1}^{3n-6} \hat{P}_j^\alpha \right\rangle, \tag{15}$$

Alternatively, the value of I_j can be obtained also by an integration of $D_j(\omega)$ over frequency.[29] With the sum rule given in Eq. (12), one can express I_j in another form as

$$I_j = \frac{1}{3n-6}(3 - P_j^T - P_j^R), \tag{16}$$

where the translational and rotational projections $P_j^T \equiv \langle \hat{P}_j^T \rangle$ and $P_j^R \equiv \langle \hat{P}_j^R \rangle$ are the ensemble averages of $\hat{P}_j^T$ and $\hat{P}_j^R$ of atom j, respectively. The I_j in Eq. (16) is thus cast into a form readily related to the translational and rotational projections of the INMs. In the event that a cluster experiences no external force, the P_j^T value is constant for all cluster configurations. In this case, I_j is simply related to the negative of the rotational projection P_j^R.

C. Order parameter

According to our previous studies for $Ag_{17}Cu_2$,[29] the I_j values of an n-atom cluster may be classified according to the point group character of the cluster structure at the LES. The group character of the lowest energy structure is well identi-

fied so that the I_j values of all atoms may be split into a number of branches each of which corresponds to a subgroup of the structure. At low temperatures, the cluster structures are near the LES and hence the I_j values are almost unchanged. As the temperature is increased, to say an intermediate temperature, the atoms in the cluster may have undertaken dynamical site permutations or the cluster is thermally driven into higher excited states. In either case, the group characters of cluster structures are different from that of the LES. In this temperature range, nevertheless, one may still recognize the split of the I_j values into branches. These I_j values start in fact to mix after a further rise in temperature and gradually they lose their original discernible branches as the temperature is raised higher and higher. Eventually, the I_j branches completely disappear and merge indistinguishably at certain temperature, say T_m, indicating that the positions of atoms in the cluster are completely dislocated. The T_m is naturally referred to as the melting temperature of the cluster. At $T > T_m$, the cluster can thus be looked upon as in a liquid-like state.

By considering a pure cluster of n atoms, the melting phenomenon described above can be quantified by an order parameter $\tau(T)$ which is defined as the standard deviation $\sigma_I(T)$ of the I_j values at a temperature T normalized by $\sigma_I(0)$ at $T = 0$, i.e.,

$$\tau(T) = \frac{\sigma_I(T)}{\sigma_I(0)} \tag{17}$$

with

$$\sigma_I(T) = \sqrt{\overline{I_j^2} - (\overline{I_j})^2} \tag{18}$$

and

$$\overline{I_j^\ell} = \frac{1}{n} \sum_{j=1}^n I_j^\ell, \tag{19}$$

where $\ell = 1$ or 2 and the bar notation in Eq. (19) denotes an arithmetic average over atoms in a cluster. Physically, the order parameter $\tau(T)$ is a quantity measuring the ordering of a cluster's structures at a finite temperature relative to its LES. At low temperatures, atoms generally vibrate about the equilibrium positions of the LES so that the value of $\tau(T)$ is of the order of unity. As the structure of a cluster becomes liquid-like at a high temperature, $\tau(T)$ approaches to an extremely small value due to the finite size of the cluster.

Inspired by Eq. (16), one may write the order parameter $\tau(T)$ in an alternative expression in terms of the rotational projection P_j^R, viz.,

$$\tau(T) = \frac{\sigma_R(T)}{\sigma_R(0)}, \tag{20}$$

where

$$\sigma_R(T) = \sqrt{\overline{\left(P_j^R\right)^2} - \left(\overline{P_j^R}\right)^2} \tag{21}$$

with

$$\overline{P_j^R} = \frac{1}{n} \sum_{j=1}^n \langle \hat{P}_j^R \rangle \tag{22}$$

and

$$\overline{\left(P_j^R\right)^2} = \frac{1}{n}\sum_{j=1}^{n}\left\langle \hat{P}_j^R\right\rangle^2. \tag{23}$$

Equations (22) and (23) involve two averages; the values of $\overline{P_j^R}$ and $\overline{(P_j^R)^2}$ are obtained by first averaging over cluster configurations and then over atoms in a cluster. Here we remark that, in principle, the $\hat{P}_j^R$ of a cluster configuration is calculated with the INM eigenvectors of (L_1, L_2, L_3) based on *Method II* given in Subsection III A. However, by replacing the three INM eigenvectors with those purely rotational eigenvectors given in Eq. (6), a reasonable approximation of the rotational projection operator reads

$$\hat{P}_j^R \approx \sum_{\eta=x,y,z}\left|\vec{e}_j^{R_\eta}\right|^2$$
$$= \frac{I_{jx}}{I_x} + \frac{I_{jy}}{I_y} + \frac{I_{jz}}{I_z}, \tag{24}$$

in which

$$I_{j\mu} = m\left(r_{j\nu}'^2 + r_{j\eta}'^2\right) \tag{25}$$

with $\mu \neq \nu \neq \eta$ assuming cyclic in x, y, and z as before. In Eq. (24), $\hat{P}_j^R$ has therefore been approximated as a sum of three ratios and each ratio measures the contribution of the atom j in the moment of inertia of a cluster's configuration with respective to one of its principal axes. By substituting this approximate $\hat{P}_j^R$ into Eqs. (22) and (23), $\overline{P_j^R}$ and $\overline{(P_j^R)^2}$ can be shown explicitly as

$$\overline{P_j^R} \approx \frac{1}{n}\sum_{j=1}^{n}\left\langle \frac{I_{jx}}{I_x} + \frac{I_{jy}}{I_y} + \frac{I_{jz}}{I_z}\right\rangle, \tag{26}$$

$$\overline{\left(P_j^R\right)^2} \approx \frac{1}{n}\sum_{j=1}^{n}\left\langle \frac{I_{jx}}{I_x} + \frac{I_{jy}}{I_y} + \frac{I_{jz}}{I_z}\right\rangle^2. \tag{27}$$

When the approximate $\overline{P_j^R}$ and $\overline{(P_j^R)^2}$ are applied to calculate the standard deviation $\sigma_R(T)$ in Eq. (21), we are led to an approximate analytic expression of the order parameter $\tau(T)$. The calculation using this analytical expression for $\tau(T)$ is certainly numerically straightforward.

We remark, furthermore, two advantages in using the approximate $\tau(T)$: (a) Theoretically, $\tau(T)$ has been reduced to a geometric one which is more directly related to the cluster structure, and (b) the computations of $\tau(T)$ are considerably easier and simplified by the unnecessity of dealing with the Hessian matrix and subsequent diagonalization. Although the approximate $\tau(T)$ is simply related to the cluster structures, the concept of the order parameter $\tau(T)$ nevertheless has its origin coming from the curvatures of potential energy landscape, which are more fundamental for they contain the dynamic information and determine the structural transition of a cluster.
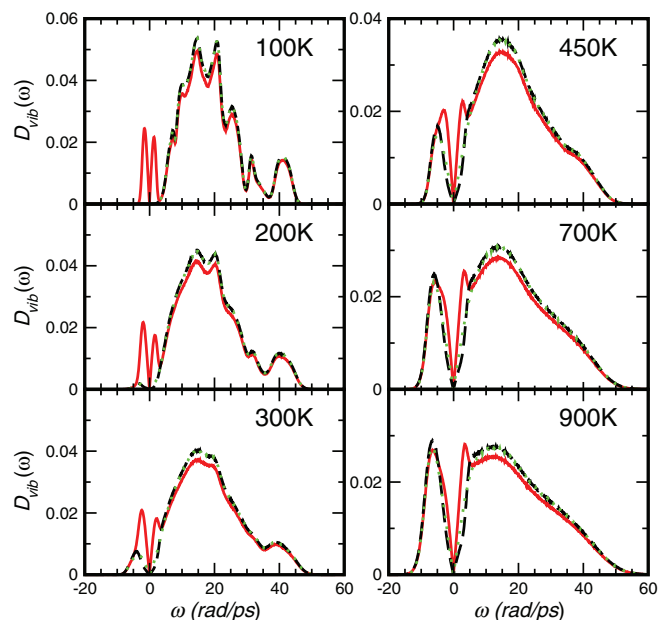

FIG. 3. Normalized INM spectra $D_{Vib}(\omega)$ of Ag$_{14}$ at 100, 200, 300, 450, 700, and 900 K. The red-solid lines are the spectra showing the contributions of both rotations and vibrations. The back-dashed and green-dotted lines are the spectra obtained by removing the rotational contribution following Method I and Method II described in the text, respectively.

IV. RESULTS AND DISCUSSION

A. INM spectra

A total number of 10^6 configurations was generated by the Brownian-type MD simulations that run at a time step of 1 fs corresponding to a total time interval of 100 ns. Figure 3 depicts the normalized INM vibrational spectra of Ag$_{14}$, obtained by subtracting the contribution of the rotational INMs described in Sec. III A by two methods. From low to high temperatures, we find no noticeable difference in the vibrational spectra obtained by the *Method I* and *Method II*. On the other hand, in order to examine the difference between the orthogonal rotational eigenvectors determined by the two methods, we calculate the projection $J(L_k)$ of the INM eigenvectors derived from (L_1, L_2, L_3) onto the subspace spanned by the three purely rotational eigenvectors. The results are presented in Fig. 4, which shows how the overlap of the subspaces spanned by the two sets of rotational eigenvectors varies with temperature. Undoubtedly, the two subspaces completely overlap at zero temperature and still overlap to a large extent at low temperatures. Among the three INMs of (L_1, L_2, L_3), the L_1 and L_3 modes have the largest and least values of $J(L_k)$ at all temperatures, respectively. The overlap of the two subspaces is significantly reduced at high temperatures: At $T = 1500$ K, $J(L_1)$ roughly lowers to 70% and $J(L_3)$ to 45%, implying a stronger coupling for the rotation-vibration at high temperatures. Based on this observation, we confine our discussion in the following to only the vibrational INM spectra calculated by *Method II*. However, for I_j and $\tau(T)$, which require the INM eigenvectors, we will touch on these quantities appealing to *Method I* or/and *Method II* for the purpose of comparison.
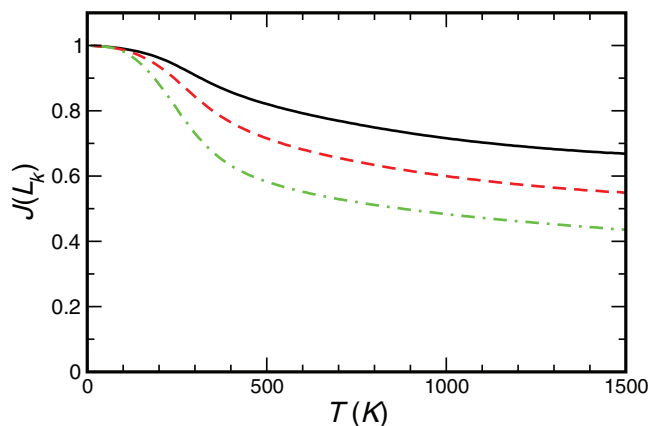
FIG. 4. Temperature variation of $J(L_k)$ for measuring the projection of the INM with L_k onto the subspace spanned by the three purely rotational eigenvectors. The black-solid, red-dashed, and green-dotted-dashed lines are for the INM with L_1, L_2, and L_3, respectively.

Coming back to Fig. 3, the $D_{Vib}(\omega)$ of Ag_{14} at $T = 100$ K possesses only the real-frequency lobe, indicating that the cluster displays by and large a solid-like characteristic. Examining closely the cluster configurations at this temperature, we find that they are still around the LES of the potential energy landscape, preserving generally the structure in the LES. It is instructive to dig out the relation between the vibrational spectral and the symmetry of cluster structure. To this end, we define as in Sec. II C, the average vibrational spectrum of a subset X of atoms, denoted by $D_X(\omega)$, by the formula

$$D_X(\omega) = \frac{1}{n_X} \sum_{j=1}^{n_X} D_j(\omega), \qquad (28)$$

where n_X is the total number of atoms in any one of the six subsets C, F, S_1, S_2, S_3, and S_4 (see Fig. 1). The structural information in $D_X(\omega)$ reflects the effects of cluster symmetry on the vibrational spectrum. The comparison between $D_X(\omega)$ at 100 K and that of the LES is given in Fig. 5. The $D_X(\omega)$ spectra of the C atom at 100 K have two main distributions whose positions of peaks are at $\omega \approx 17$ and 41.5 rad/ps coinciding with the thin straight lines of $D_X(\omega)$ at 0 K. Hence, the spectra of $D_X(\omega)$ at 100 K are the consequence of the thermal effect driving the cluster structure to deviate from the LES of the potential energy landscape. The spectrum of the F atom has three main peaks at $\omega \approx 7$, 11.2, and 34 rad/ps, a plateau around 20 rad/ps, and almost without any mode with $\omega > 40$ rad/ps. Among these the peaks at 7 and 34 rad/ps are related to the shearing and stretching vibrations between the F atom and the deformed icosahedron, respectively. For the subsets of S_1, S_2, S_3, and S_4, an ubiquitous feature of their $D_X(\omega)$ is a continuous frequency distribution that extends the range $\omega \approx 5$–45 rad/ps with a deep valley around 36 rad/ps. Scrutinizing these four spectra in great details, we find their $D_X(\omega)$ around 31 rad/ps at which the breathing mode occurs in the LES have an almost equal magnitude. On the other hand, one can tell apart the difference between the spectrum of the S_1 subset, which directly links to the F atom, and those of the other S_i ($i = 2, 3, 4$) subsets. At $T = 0$ and 100 K, the $D_X(\omega)$ spectrum of the S_1 subset has a relatively larger magnitude at
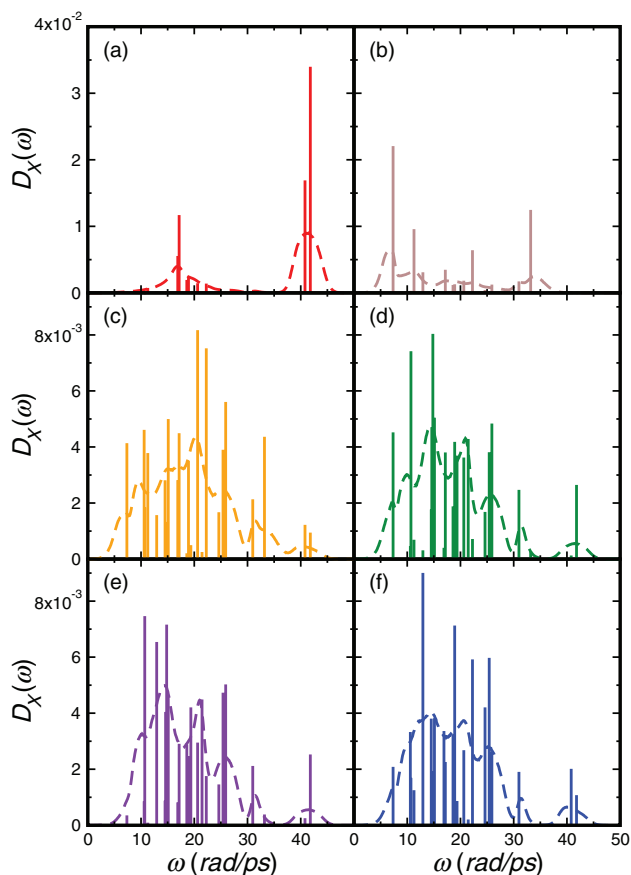

FIG. 5. Vibrational DOSs, $D_X(\omega)$, of subset X of Ag_{14}, with (a) $X = C$, (b) $X = F$, (c) $X = S_1$, (d) $X = S_2$, (e) $X = S_3$, and (f) $X = S_4$. The six subsets are referred to in Fig. 1. In each panel, the thin straight lines are for the LES and the dashed curve is an ensemble average over cluster configurations at 100 K.

around 34 rad/ps than the other three subsets. However, both $D_X(\omega)$ of the S_1 and S_2 subsets have almost equal magnitude at $\omega \approx 7$ rad/ps, which is larger than those of the S_3 and S_4 subsets. These results point to the quite general feature that the stretching vibration between the F atom and the deformed icosahedron only extends to atoms of the S_1 subset but the shearing vibration extends further to those of the S_2 atoms.

To explore further the temperature effect on the INM vibrational spectrum of individual atom in Ag_{14}, we display in Fig. 6 the variations of $D_j(\omega)$ from 50 to 1000 K for all atoms. At 50 K, the structural characteristics of $D_j(\omega)$ are well discernible for the C, F, and S_i atoms. Up to 100 K, the $D_j(\omega)$ spectra do not contain any imaginary-frequency INM and are rather similar to the power spectra obtained by the Fourier-transform of the velocity autocorrelation functions of individual atoms presented in Ref. 30. The $D_j(\omega)$ of the surface atoms are generally indiscernible at 150 K, and they are seen to merge with the spectrum of the F atom at 200 K into an almost single spectrum, with the appearance of some imaginary-frequency modes and weak structures in the real-frequency lobe. This mergence of $D_j(\omega)$ indicates that the F atom has indistinguishably integrated with the surface atoms at 200 K. For temperature higher than 200–400 K, only two kinds of distinguishable $D_j(\omega)$ spectra are observed and they come from the C-atom and the rest of atoms. However, some
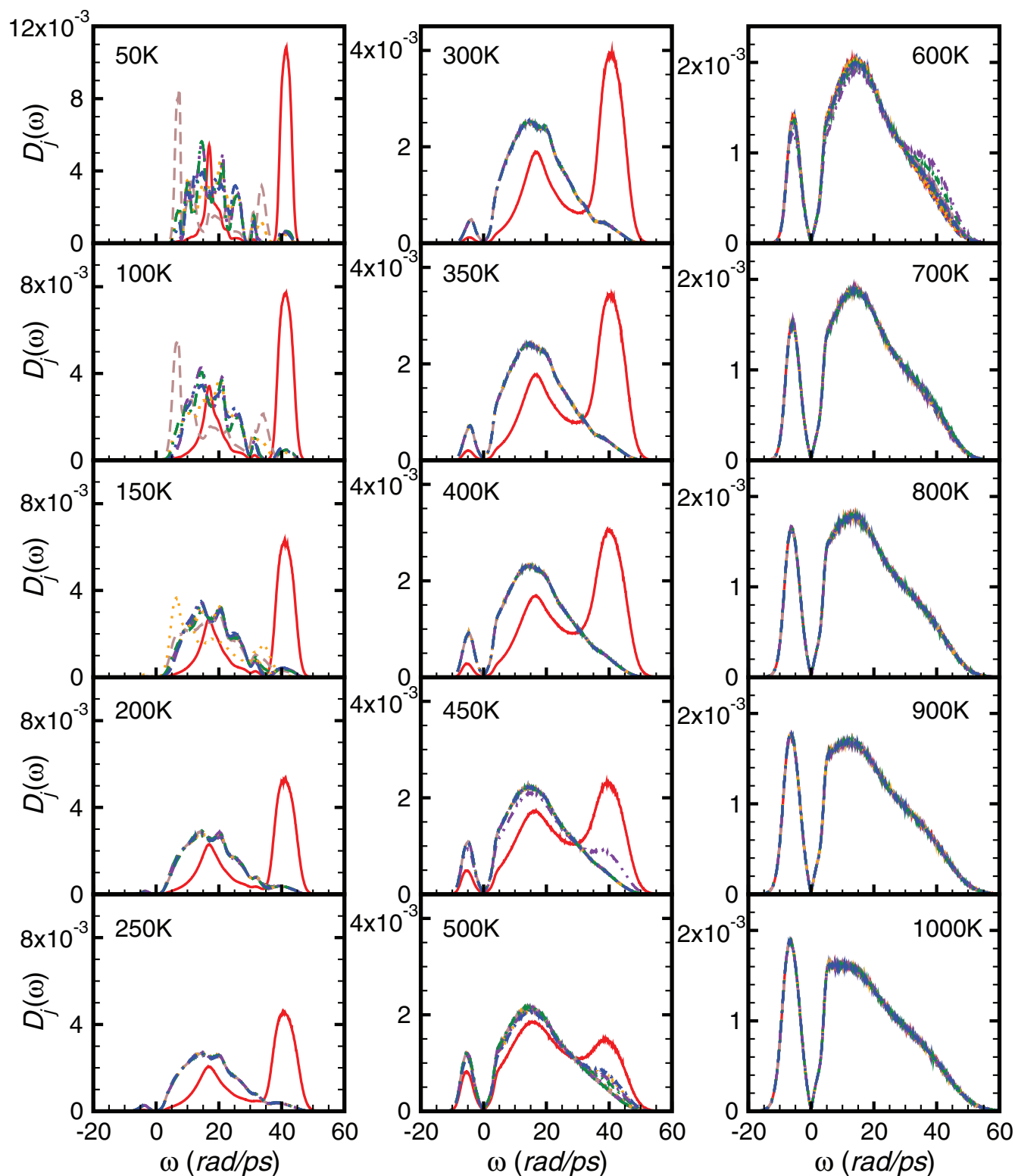
FIG. 6. INM vibrational spectra $D_j(\omega)$ of individual atoms at indicated temperatures. The spectra are obtained by following *Method II*. The solid (red) and dashed (brown) lines are for the C and F atoms, respectively. The dotted (orange), dotted-dashed (green), dotted-dotted-dashed (violet), and dotted-dashed-dashed (blue) lines refer to the atoms of the S_1, S_2, S_3, and S_4 subsets, respectively.

interesting things happen at 450 K. Discernible from other subsets as well, the $D_j(\omega)$ spectra of the S_3 atoms clearly show a shoulder at 40 rad/ps, a value close to the frequencies of the C-atom oscillating inside the cage of the deformed icosahedron in the LES. The occurrence of the shoulder suggests that

at this temperature there is some possibility for the S_3 atoms to occupy the central position of the deformed icosahedron. When entering into 500 K, the $D_j(\omega)$ of the C-atom is still separated from those of the rest of atoms. At this temperature its high-frequency peak is located at around 40 rad/ps but

shifts slightly toward smaller frequency accompanying by a decline in amplitude. In contrast, the originally merged $D_j(\omega)$ of the rest of atoms are somewhat blurred and have a conspicuous hump falling in the frequency range of the shoulder observed in the spectra of the S_3 atoms at 450 K. As the temperature goes up further to 600 K, the $D_j(\omega)$ spectra of all atoms, including the C-atom, are mixed up. In fact, one still detects a weak hump on the high-frequency side at $\omega \approx 40$ rad/ps. The occurrence of this high-frequency hump demonstrates that the structure of the cluster at this temperature still has an atom centrally resided inside the cage formed by other atoms but this central atom may not be the C-atom. The hump disappears for $T > 600$ K and all $D_j(\omega)$ spectra are seen to coalesce and display a large portion of imaginary-frequency INMs, whereas the real-frequency lobe develops into a roughly triangular shape that is often observed in the INM spectra of simple liquids.[42,43] These characteristics of $D_j(\omega)$ are reminiscent of $Ag_{17}Cu_2$ in the liquid-like phase and point to same behaviors of Ag_{14} whose atoms at such high temperatures would have gone around everywhere the potential energy landscape.[29]

B. Temperature variation of I_j

The temperature variations of the I_j values for all atoms are presented in Fig. 7. With a temperature increment of 10 K from $T = 10$ up to 1500 K, the data at each T are calculated by averaging over 10^6 configurations. In the upper panel of Fig. 7, the I_j values of the six subsets of atoms are specified by different symbols and they are obtained by an integration of each $D_j(\omega)$ curve (see Fig. 6) with the vibrational INMs described by the *Method II*. In the lower panel of Fig. 7, we make a comparison between the I_j values obtained by two different methods, one via the integral of $D_j(\omega)$ and the other via Eq. (16) in which the translational projection is calculated straightforwardly and the rotational projection is evaluated with the purely rotational eigenvectors given in Eq. (6). As evidenced in Fig. 7, the two methods for the six subsets of atoms yield rather similar results in I_j.

Let us look first at the lower panel of Fig. 7. One sees that the I_j curves of all atoms below 150 K are well split into six branches, with each branch corresponding to a subset of atoms. The six branches show that the LES is well preserved. For the F and C atoms, it is easy to understand their branches as due to their unique positions in the LES, whereas for the four S_i subsets of atoms, it is, however, relatively less simple to interpret the splitting of their I_j branches as connecting to the geometry of the deformed icosahedron. To delve more deeply into the I_j branches, we examine Fig. 7 more closely. First of all, we find that between 100 and 150 K the F atom declines weakly in the I_j value obtained by *Method II*. What happens to the F atom in this temperature range is that the atom possibly relocates from a triangular facet to a nearby one by migrating over their common edge. This mechanism is shown in Fig. 8 by a potential energy barrier which is estimated to be 97 K.[52] These migration and relocation movements of the F atom were previously observed also in Cu_{14}.[11] Furthermore, we find exchanges in the I_j values among the F
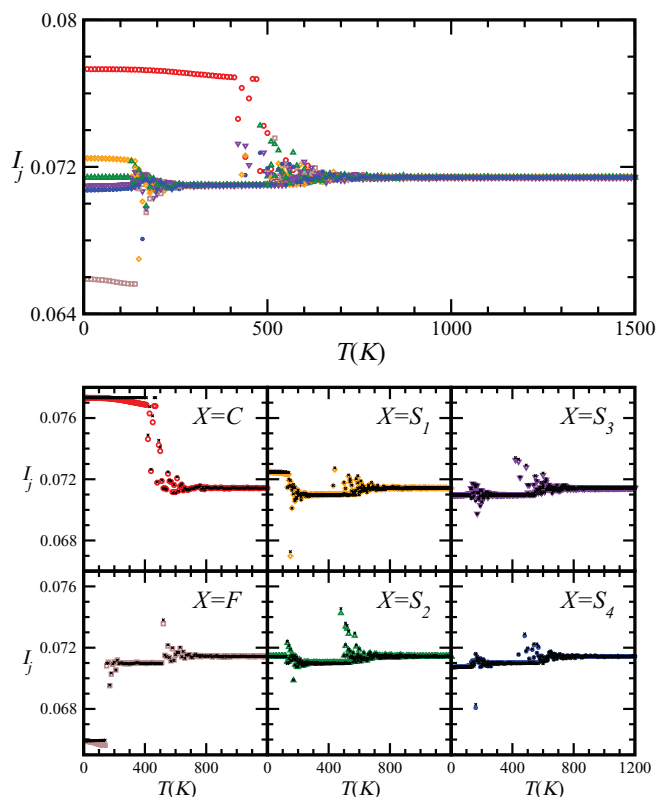

FIG. 7. Temperature variations of I_j with atoms specified by the six subsets: $X = C$ (red circles), $X = F$ (brown squares), $X = S_1$ (orange diamonds), $X = S_2$ (green upper-triangles), $X = S_3$ (violet down-triangles), and $X = S_4$ (blue stars). In the upper panel, the I_j value is the integral of $D_j(\omega)$ shown in Fig. 6. Each figure in the lower panel compares the integral I_j value of a subset of atoms and the corresponding value obtained via Eq. (16) with the approximate rotational projection operator given in Eqs. (24) and (25) (black crosses).

and the S_i atoms spanning the temperature range 150–200 K. These exchanges can be understood by a mechanism shown in Fig. 9(b), where the role of the F atom as one floating outside the deformed icosahedron is replaced by one S_1 atom with the occurrence of site exchanges among other S_i atoms.[53] The overall potential energy barrier in this mechanism is about 127 K. At temperatures higher than 200 K, the five branches of the subsets of F and S_i atoms show tendency to coalesce and become completely indiscernible at $T \approx 300$ K. Dynamically, this would correspond to the picture that the F atom seeps into the deformed icosahedron and merges with the S_2, S_3, and S_4 atoms. The complete merger of the five branches at around 300 K implies that the structure of Ag_{14} possesses no more floating atom but a central atom plus its surrounding 13 atoms. This latter temperature corresponds to the position of the prepeak observed in the C_V curve.[30]

At temperatures up to 400 K, the I_j branch of the C-atom is clearly well separated from the branches of other subsets of atoms. Structurally, this manifests the solid-like behavior of the C-atom being remained at the center of the cluster. Between 400 and 500 K, the I_j value of the C-atom is observed to drop in a scattered manner. This thermal behavior is apparently opposite to the increase in the I_j value of the S_3 atoms and may be traced to the contribution from the high-frequency shoulder in the $D_j(\omega)$ spectra at 450 K (see Fig. 6). This
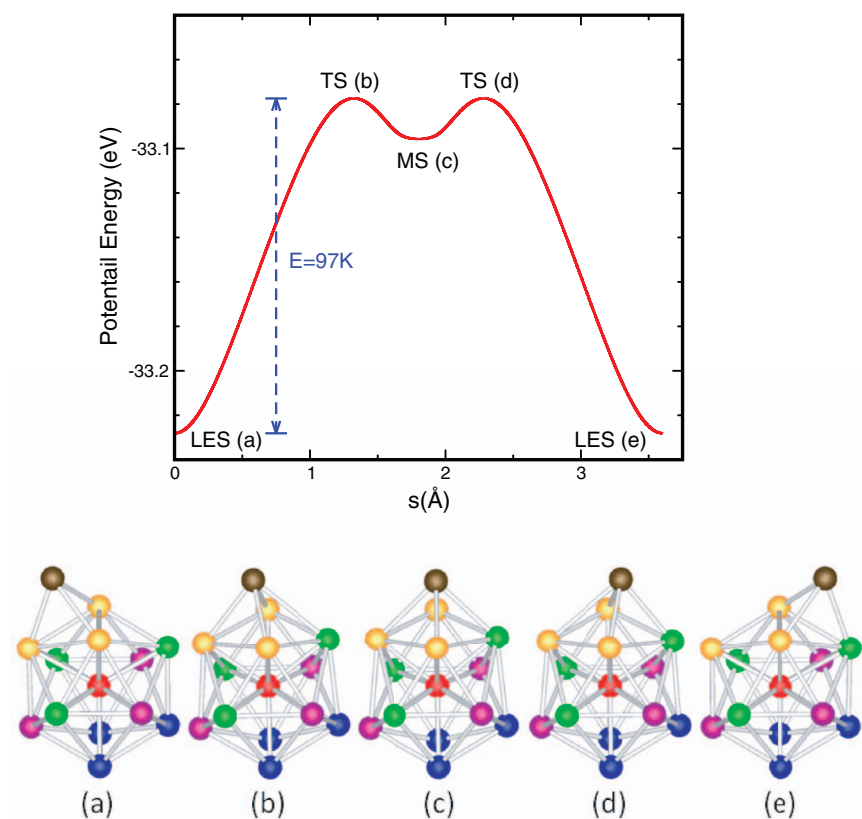
FIG. 8. The potential energy (red curve) as a function of the integrated path length s for a two-step path via two transition states, (b) and (d), and one metastable state (c) of Ag_{14}. The path connects to the two LESs, (a) and (e). Along the path, shown in the lower part, the F-atom (brown) migrates between two nearby triangular facets by crossing their common edge. In the LES (a), the F atom links to three S_1 (orange) atoms; in the LES (e), the F atom links to two S_1 atoms and one S_2 (green) atom. The metastable state (c) is a first excited state of the cluster.[30] The transition state (b) is found by using the OPTIM program[46–48] from the LES (a) as the Hessian matrix possesses a unique negative eigenvalue. The path from (a) to (c) is obtained by using the steepest-decent algorithm[49] with the starting point chosen at (b) along the two opposite directions of the eigenvector corresponding to the unique negative eigenvalue. The transition state (d) and the path from (e) to (c) are obtained similarly. Note that the potential energy is calculated along the steepest-decent path[50,51] and the potential energy barrier from (a) to (b) is estimated to be 97 K.

suggests furthermore that the structure of the cluster in this temperature range still maintains a firm "solid-state" center, even though the C-atom has a preference to dynamically permute its site with any of the S_3 atoms. The I_j branches of all atoms start to mix at temperatures above 500 K and gradually lose the identities of their original subsets. The panorama of the I_j branches described here is reminiscent of the premelting of the F-atom into the surface atoms at $T \approx 300$ K. As the temperature goes up much higher, the I_j branches of all atoms completely align into one single value, exhibiting a picture of complete indistinguishability of atoms and the cluster by now is appropriately described as a liquid-like phase.

C. Order parameter $\tau(T)$ for cluster melting

We show in Fig. 10, the order parameters $\tau(T)$ calculated with either the I_j values according to Eqs. (17)–(19) or the average values of the rotational projection by employing the purely rotational eigenvectors according to Eqs. (20), (21), (26) and (27). A glimpse of Fig. 10 shows that the $\tau(T)$ obtained by the two methods are strikingly similar except in the region between 200 and 500 K. The correspondence between $\tau(T)$ and C_V[30] can be made by comparing them side by side.

Below 150 K, $\tau(T)$ is almost one, reflecting the small-amplitude vibrations of atoms around the LES and these vibrations result in a mild increase in C_V with temperature. It is interesting to see that $\tau(T)$ undergoes a sudden decline between 150 and 200 K, which may be interpreted as the migration and relocation of the F-atom near the surface of the deformed icosahedron[11,30] or site-permutations between the F atom and the surface atoms. The significant jump of $\tau(T)$ from 1 to 0.70 corresponds to the first sharp rise in C_V at 150 K before the prepeak. Following this jump, the behavior of $\tau(T)$ in the temperature window 200–450 K has a small decrease by the method with the integral I_j values, which contrasts to the constant values by the purely rotational eigenvectors. Physically, this temperature region marks the dissolution of the F-atom into the surface of the deformed icosahedron. The almost flat region of $\tau(T)$ thus has intimate relevance to the prepeak structure of C_V, with the middle of the flat region roughly matching the prepeak position of C_V at $T \approx 300$ K.

The behaviors of $\tau(T)$ and C_V beyond the temperature region mentioned above are rather similar to those for $Ag_{17}Cu_2$. First, we see a sharp drop in the $\tau(T)$ of Ag_{14} around 500 K, at which temperature a second sharp rise in C_V occurs. As the temperature is raised above 500 K, we see another
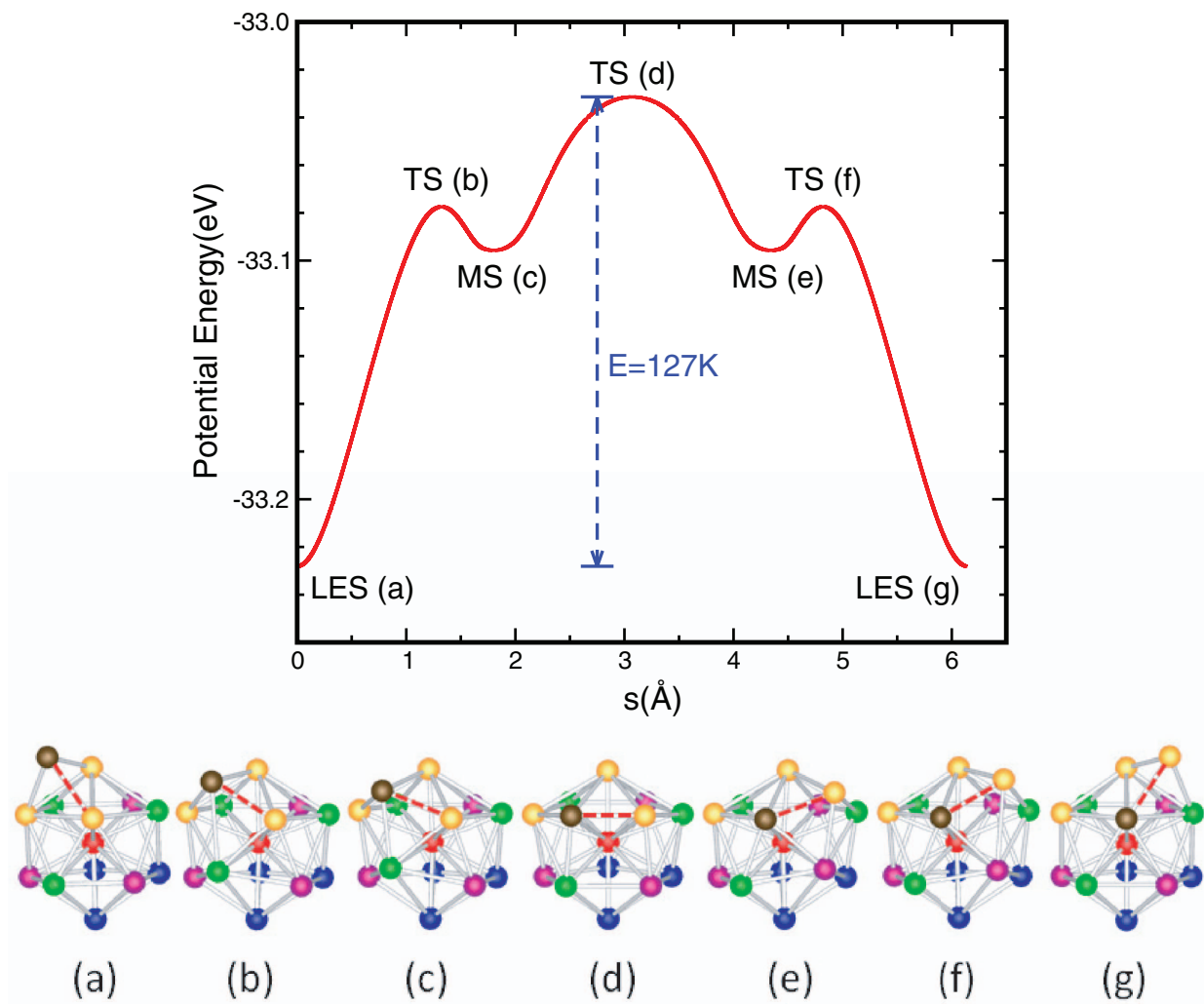
FIG. 9. The potential energy (red curve) as a function of the integrated path length *s* for a three-step path via three transition states, (b), (d), and (f), and two metastable states, (c) and (e), of Ag_{14}. The path connects to the two LESs, (a) and (g). The low part illustrates the path for the mechanism of site-permutation between the *F* (brown) and one of S_1 (orange) atoms, which are linked by a dashed red line. In the LES (a), the *F* atom is the one floating outside the deformed icosahedron, whereas in the LES (g), the floating atom has been replaced by one of S_1 atoms. The (c) and (e) are the two first excited states of the cluster.[30] The three transition states and the path are obtained by the method as described in Fig. 8. Similar as in Fig. 8, the potential energy is calculated along the path and the potential energy barrier from (a) to (d) is estimated to be 127 K.
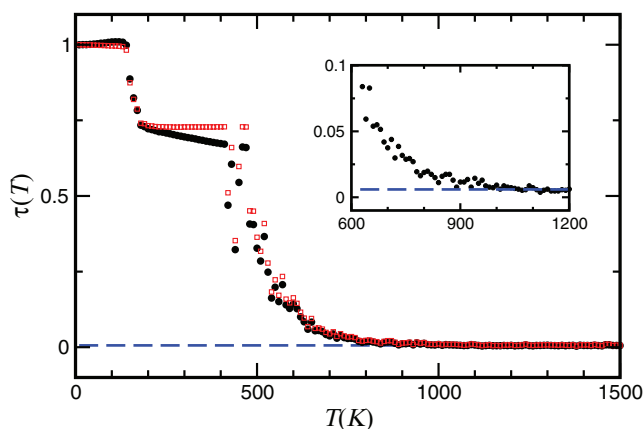

FIG. 10. Temperature variation of order parameter $\tau(T)$ for Ag_{14} cluster. The filled circles are calculated via Eqs. (17) and (18) with the integral I_j values shown in Fig. 7 and the open squares are obtained via Eqs. (20) and (21) with the approximate rotational projections given in Eqs. (26) and (27). The dashed line indicates the values of $\tau(T)$ above 1000 K. The inset enlarges $\tau(T)$ function for better visualization of the thermal behavior of $\tau(T)$ near 900 K.

drastic change of $\tau(T)$. A conspicuous characteristic of $\tau(T)$ is its abrupt drop and approaches asymptotically to a small value (see the inset in Fig. 10) at a temperature close to 920 K. The latter is strikingly close to the position of the main peak of C_V. This temperature range thus describes the mixing process of the central atom with its surrounding atoms, where the cluster is driven thermally into configurations of higher energy excited states. The behavior of the sudden decline in $\tau(T)$ of Ag_{14} is also observed in $Ag_{17}Cu_2$. Both clusters point to a transition during which the solid-like and liquid-like isomers coexist. At temperatures above T_m, the finite size of the cluster yields a small non-zero constant $\tau(T)$ value, which suggests no further distinction among the atoms in the cluster; correspondingly, C_V decays with increasing temperature. The cluster at this moment behaves more liquid-like.

In recapitulation, we demonstrate with concrete illustrations for the present results of Ag_{14} and preceding work for $Ag_{17}Cu_2$ that $\tau(T)$ is an insightful order parameter capable of describing consistently the phenomenon of cluster melting

and its intimate relevance to the thermal variation of C_V even for clusters containing a prepeak and a main peak.

V. CONCLUDING REMARKS

We have performed isothermal Brownian-type MD simulations with the Gupta potential for Ag_{14} that was carried out for temperatures up to 1500 K. At each temperature, we recorded a total number of 10^6 configurations and these were subsequently used to investigate the phenomenon of cluster melting and its relevance to the prepeak and main peak structures of C_V. Methodologically, we used the INM analysis, which was developed previously[37–39] for clusters in general and recently extended by us[29] to study the melting behavior of $Ag_{17}Cu_2$ whose C_V exhibits only a single main peak. There, an order parameter $\tau(T)$ was defined as the normalized standard deviation of the integral I_j of the INM vibrational DOSs associated with the Ag atoms.[29]

In this paper, we address further the $\tau(T)$ defined in the INM approach. The integral I_j value of a pure cluster is found to be related to the rotational projection of the jth atom in the cluster, where the projection consists of a sum of three ratios with each ratio measuring the ensemble-averaged contribution of the atom in the moment of inertia of the whole cluster calculated with respect to one of its principal axes. Thus, the order parameter $\tau(T)$ can be defined in a scheme associated with the vibrational motions of individual atoms or the rotational motion of the whole cluster assuming to be rigid. We demonstrate that almost equivalent results were obtained by the two definitions of $\tau(T)$ for Ag_{14}. Physically, the description of the melting for Ag_{14} by $\tau(T)$ agrees very well with that inferred from C_V. Our present and previous results strengthen our belief that $\tau(T)$ is an order parameter that sheds considerable light on cluster melting and provides a means to ravel the microscopic dynamics of clusters from the point of view of potential energy landscape.

The reason why the order parameter $\tau(T)$ works so well is not fortuitous but stems from the fact that the I_j values are fundamentally related to the symmetry of the cluster structures at different temperatures. The split of I_j values at lower temperatures into several branches follows the symmetry of the LES of a cluster according to the group theory. At high temperatures, the I_j values merge into one since the cluster configurations stray far from its LES resulting in the loss of symmetry. It is well known in condensed matter physics that the phase transition in bulk systems from a crystal to a liquid is described by the concept of broken symmetry.[54] The present results of the I_j values imply that the broken symmetry is also a useful concept for understanding the melting of clusters. The main difference in the melting transition between clusters and bulk systems lies in the extent of the symmetry breaking: For bulk systems, the broken symmetry is associated with an infinite number of degrees of freedom so that the transition is abrupt at a melting temperature, whereas in clusters the symmetry broken is associated with a finite number of degrees of freedom so that the transition is gradual and, therefore, occurring within a temperature interval. The quantitative estimate for the broken symmetry during cluster melting would have to refer to a similar discussion of examining

the distance of a distorted molecule from any chosen element of symmetry.[55]

By following the concept of broken symmetry, it is worth re-thinking of why the C_V of Ag_{14} has an additional prepeak, whereas none in $Ag_{17}Cu_2$. Based on our studies so far, we conjecture that the plausible reason is probably related to the difference in the LESs of the two clusters: The structure of $Ag_{17}Cu_2$ has a C_5 rotational axis symmetry that passes through the Cu central atoms while that of Ag_{14}, with a floating atom outside a deformed icosahedron, possesses only the rotational symmetry about its principal axis. According to our findings, the prepeak of C_V seen in Ag_{14} is associated with the dissolution of the floating atom into the surface of the deformed icosahedron so that the structures of Ag_{14} change to ones with a stabilized central atom which is surrounded by the rest of the atoms. Accordingly, the cluster melting at higher temperatures is associated with the symmetry breaking as the structural center is being destroyed by the thermal motion of atoms, similar to that for $Ag_{17}Cu_2$. As far as the cluster melting is concerned, it would be intriguing to examine melting transition with the concept of broken symmetry especially between clusters whose LESs have different structural symmetries. On the other hand, an INM investigation for the temperature variation of the imaginary-part contribution during melting transition of clusters is another interesting issue for our future work.

[1]D. J. Wales, *Energy Landscapes, with Applications to Clusters, Biomolecules and Glasses* (Cambridge University Press; Cambridge 2003).
[2]Y. Imry, Phys. Rev. B **21**, 2042 (1980).
[3]A. Hüller, Z. Phys. D **95**, 63 (1994).
[4]M. Schmidt, R. Kusche, W. Kronmüller, B. von Issendorff, and H. Haberland, Phys. Rev. Lett. **79**, 99 (1997).
[5]M. Schmidt, R. Kusche, B. V. Issendorff, and H. Haberland, Nature (London) **393**, 238 (1998).
[6]H. Schmidt and H. Haberland, C.R. Phys. **3**, 327 (2002).
[7]C. M. Neal, A. K. Starace, and M. F. Jarrold, Phys. Rev. B **76**, 054113 (2007).
[8]B. Cao, A. K. Starace, C. M. Neal, M. F. Jarrold, S. Núñez, J. M. López, and A. Aguado, J. Chem. Phys. **129**, 124709 (2008).
[9]B. Cao, A. K. Starace, O. H. Judd, I. Bhattacharyya, and M. F. Jarrold, J. Chem. Phys. **131**, 124305 (2009).
[10]T. W. Yen, S. K. Lai, N. Jakse, and J. L. Bretonnet, Phys. Rev. B **75**, 165420 (2007).
[11]P. J. Hsu, J. S. Luo, S. K. Lai, J. F. Wax, and J. L. Bretonnet, J. Chem. Phys. **129**, 194302 (2008).
[12]J. Jellinek, T. L. Beck, and R. S. Berry, J. Chem. Phys. **84**, 2783 (1986).
[13]T. L. Beck, J. Jellinek, and R. S. Berry, J. Chem. Phys. **87**, 545 (1987).
[14]T. L. Beck and R. S. Berry, J. Chem. Phys. **88**, 3910 (1988).
[15]D. J. Wales, J. Chem. Soc., Faraday Trans. **87**, 2399 (1991).
[16]J. D. Honeycutt and H. C. Andersen, J. Phys. Chem. **91**, 4950 (1987).
[17]R. M. Lynden-Bell and D. J. Wales, J. Chem. Phys. **101**, 1460 (1994).
[18]J. P. K. Doye and D. J. Wales, J. Chem. Phys. **102**, 9673 (1995).
[19]D. J. Wales, J. Chem. Phys. **101**, 3750 (1994).
[20]F. Calvo, Phys. Rev. E **82**, 046703 (2010).

[21]L. Zhan, J. Z. Y. Chen, and W. K. Liu, J. Chem. Phys. **127**, 141101 (2007).

[22]M. Picciani, M. Athènes, J. Kurchan, and J. Tailleur, J. Chem. Phys. **135**, 034108 (2011).

[23]F. Calvo and F. Spiegelmann, J. Chem. Phys. **112**, 2888 (2000).

[24]S. K. Lai, W. D. Lin, K. L. Wu, W. H. Li, and K. C. Lee, J. Chem. Phys. **121**, 1487 (2004).

[25]F. H. Stillinger and T. A. Weber, Phys. Rev. A **25**, 978 (1982); **28**, 2408 (1983).

[26]F. H. Stillinger and T. A. Weber, Science **225**, 983 (1984).

[27]R. M. Stratt, Acc. Chem. Res. **28**, 201 (1995).

[28]T. Keyes, J. Phys. Chem. A **101**, 2921 (1997).

[29]P. H. Tang, T. M. Wu, T. W. Yen, S. K. Lai, and P. J. Hsu, J. Chem. Phys. **135**, 094302 (2011).

[30]T. W. Yen, P. J. Hsu, and S. K. Lai, e-J. Surf. Sci. Nanotechnol. **7**, 149 (2009).

[31]R. P. Gupta, Phys. Rev. B **23**, 6265 (1981).

[32]A. Rapallo, G. Rossi, R. Ferrando, A. Fortunelli, B. C. Curley, L. D. Lloyd, G. M. Tarbuck, and R. L. Johnston, J. Chem. Phys. **122**, 194308 (2005).

[33]P. J. Hsu and S. K. Lai, J. Chem. Phys. **124**, 044711 (2006).

[34]R. L. Carter, *Molecular Symmetry and Group Theory* (Wiley, New York, 1998).

[35]A. Posada-Amarillas and I. L. Garzón, Phys. Rev. B **54**, 10362 (1996).

[36]I. L. Garsón and A. Posada-Amarillas, Phys. Rev. B **54**, 11796 (1996).

[37]J. E. Adams and R. M. Stratt, J. Chem. Phys. **93**, 1332 (1990).

[38]J. E. Adams and R. M. Stratt, J. Chem. Phys. **93**, 1358 (1990).

[39]J. E. Adams and R. M. Stratt, J. Chem. Phys. **93**, 1632 (1990).

[40]J. Jellinek and D. H. Li, Phys. Rev. Lett. **62**, 241 (1989).

[41]M. Page and J. W. McIver, J. Chem. Phys. **88**, 922 (1988).

[42]T. M. Wu and R. F. Loring, J. Chem. Phys. **97**, 8568 (1992).

[43]Y. Wan and R. M. Stratt, J. Chem. Phys. **100**, 5123 (1994).

[44]M. Buchner, B. M. Ladanyi, and R. M. Stratt, J. Chem. Phys. **97**, 8522 (1992).

[45]R. E. Larsen, G. Goodyear, and R. M. Stratt, J. Chem. Phys. **104**, 2987 (1996).

[46]D. J. Wales, J. P. K. Doye, M. A. Miller, P. N. Mortenson, and T. R. Walsh, "Energy landscapes: From clusters to biomolecules," in *Advances in Chemical Physics*, edited by I. Prigogine and S. A. Rice (Wiley, 2000), Vol. 115, Chap. I.

[47]Y. Kumeda, L. J. Munro, and D. J. Wales, Chem. Phys. Lett. **341**, 185 (2001).

[48]S. A. Trygubenko and D. J. Wales, J. Chem. Phys. **120**, 2082 (2004).

[49]W. H. Press, S. A. Teukolsky, W. T. Vetterling, and B. P. Flannery, *Numerical Recipes in C*, 2nd ed. (Cambridge University Press, Cambridge 1992).

[50]D. J. Wales, Mol. Phys. **100**, 3285 (2002).

[51]D. J. Wales, Mol. Phys. **102**, 891 (2004).

[52]The mechanism shown in Fig. 8(b) can be elucidated further as follows: From (a) to (b), a bond that connects the F (brown) and one of S_2 (green) atoms is formed, in contrast to the breaking of the bond between the two S_1 (orange) atoms connecting to the S_2 atom. From (d) to (e), the broken bond is re-bonded, whereas the bond connecting the F and the third S_1 atoms is broken. In all calculations, the bond length is set equal 3.5 Å.

[53]The following describes the site-permutation mechanism illustrated in Fig. 9(b) for the F (brown) atom exchanging with one of S_1 (orange) atoms and, as a result, the S_1 atom playing the role as the one floating outside the deformed icosahedron. The path from (a) to (c) results in the bonding of the F atom with one of S_2 (green) atoms and the breaking of the bond between two S_1 atoms both linked to the S_2 atom. As in Ref. 52, we set two atoms as bonded when their distance is within 3.5 Å. From (c) to (d), the F and C (red) atoms are thus connected, while the S_1 and S_2 atoms that are simultaneously linked to the F atom are unbonded. From (d) to (e), the S_1 atom which is disconnected from the S_2 atom plays the role as a new floating atom after its bond with the C atom breaks up, while the F and one S_3 (violet) atoms which both connected to the new floating atom are bonded. From (f) to (g), the F and another S_2 atoms are bonded and, on the same occasion, the new floating atom is seen to be disconnected from the S_3 atom that has linked to the F atom.

[54]P. M. Chaikin and T. C. Lubensky, *Principles of Condensed Matter Physics* (Cambridge University Press, Cambridge, 1995).

[55]H. Zabrodsky, S. Peleg, and D. Avnir, J. Am. Chem. Soc. **114**, 7843 (1992).